ELSEVIER

Chemical Engineering Journal 136 (2008) 242–255

Chemical Engineering Journal

www.elsevier.com/locate/cej

Mass transfer limitations in photocatalytic reactors employing titanium dioxide suspensions II. External and internal particle constrains for the reaction

María de los Milagros Ballari, Rodolfo Brandi, Orlando Alfano, Alberto Cassano *

INTEC, Universidad Nacional del Litoral and CONICET, Güemes 3450, 3000 Santa Fe, Argentina

Received 12 October 2006; received in revised form 15 March 2007; accepted 19 March 2007

Abstract

This work is a continuation of a previous study concerning the problem of mass transfer limitations in slurry, photocatalytic reactors employing pure, titanium dioxide suspensions. With simulation experiments applied to an existing isothermal reactor, the mineralization reaction of dichloroacetic acid was used as a test reaction because introducing some corrections in the model of a published work, and resorting to the original experimental data, an intrinsic reaction kinetics was available. In the first part, only irreducible radiation field non-uniformities and the existence, under some operating conditions, of strong, mass concentration gradients in the bulk were explored. It was found that the last might be significant unless very good mixing conditions prevail. In this second part, the study is concentrated on external and internal catalytic particles (or agglomerates) transport limitations. In this case, resorting to the definition of a specifically defined photocatalytic effectiveness factor, the coupled effects of concentration gradients and light penetration impediments can be analyzed separately. The mathematical description of the catalytic particle (or agglomerate) performance is made employing rigorous, radiation and mass transfer models derived from fundamental principles. The main explored variables were (i) irradiation rates, particularly considering the influence of the wavelength distribution of the employed radiation, (ii) size of the catalytic particles and their eventual agglomerations, (iii) virtual changes in the reaction rate, to include the possibility of faster reactions, (iv) catalyst loadings and (v) porosity of the catalyst agglomeration. Only for very large particles, not usually employed with unsupported titanium dioxide, interfacial external mass transfer limitations in the boundary layer surrounding the catalytic particle may be significant. Inside the catalytic particle or the porous agglomerate, the most important restriction is the light penetration that can be observed even in particle sizes (or agglomerates) below 1 μm.

Keywords: Photocatalysis; Slurry reactors; External mass transfer limitations; Internal mass transfer limitations; Unsupported titanium dioxide

1. Introduction

Photocatalytic reactions are a promising technology for pollution remediation in water and air contaminated environments and they can be applied for a variety of compounds due their very low selectivity. One of the critical aspects that deserves a detailed analysis is the possibility of mass transfer limitations due to the characteristics imposed in the reaction space by the existence of the solid catalyst. Although, this seems to be a widely recognized problem in fixed titanium dioxide operations (either on dispersed, much larger size, solid supports or in packed bed, wall catalyzed and membrane reactors) the problem of finding analogous limitations in suspended, pure titanium dioxide has received considerably less attention. The general background of the problem at stake has been described in details in a previous contribution [1] and will not be repeated here. However, some specific reports deserve to be mentioned in this introduction. Exclusion is made of all the cases concerning immobilized titanium catalyst in different supports and configurations because they belong to a different class of problem.

Sclafani et al. [2] postulated external mass transfer limitations to describe their results in a packed bed reactor filled with spheres of pure titanium dioxide (*ca.* 0.12 cm in diameter). Chen and Ray [3] studied internal and external mass transfer limitations in catalytic particles of photocatalytic reactors considering first-order reaction for different contaminants, and explained the obtained results in terms of existence of only mild mass transfer restrictions. Employing agglomerates of 5 μm, they found

* Corresponding author. Fax: +54 342 4511087.
E-mail address: acassano@ceride.gov.ar (A. Cassano).

1385-8947/$ – see front matter © 2007 Elsevier B.V. All rights reserved.
doi:10.1016/j.cej.2007.03.031

Nomenclature

a_V	solid–liquid interfacial area per unit reactor volume ($cm^2\ cm^{-3}$)
a_{V_p}	solid–liquid interfacial area per unit particle volume ($cm^2\ cm^{-3}$)
A	area (cm^2)
c	light speed ($cm\ s^{-1}$)
C_A	molar concentration of component A ($mol\ cm^{-3}$)
C_{mc}	mass concentration of catalyst ($g\ cm^{-3}$)
C_{O_2}	molar concentration of oxygen ($mol\ cm^{-3}$)
d	diameter (nm)
$D_{A,mix}$	pseudo-binary diffusion coefficient ($cm^2\ s^{-1}$)
$D_{A,turb}$	eddy turbulent diffusion coefficient ($cm^2\ s^{-1}$)
$D_{A,eff}$	effective diffusion coefficient ($cm^2\ s^{-1}$)
e^a	local volumetric rate of photon absorption (Einstein $s^{-1}\ cm^{-3}$)
e^a_S	local superficial rate of photon absorption (Einstein $s^{-1}\ cm^{-2}$)
g	gravity ($cm\ s^{-2}$)
g	parameter in the phase function for scattering
G	incident radiation (Einstein $s^{-1}\ cm^{-2}$)
H	depth (cm)
I	specific radiation intensity (Einstein $s^{-1}\ cm^{-2}\ sr^{-1}$)
k_s	external mass transfer coefficient ($cm\ s^{-1}$)
L	length (cm)
m	mass (g)
N_p	number of particles
p	phase function
P	radiation pressure (Pa)
q	radiative flux (Einstein $s^{-1}\ cm^{-2}$)
Q	volumetric flow rate ($cm^3\ s^{-1}$)
r	radial coordinate (cm)
R	radius (cm)
R_{Het}	heterogeneous reaction rate ($mol\ s^{-1}\ cm^{-2}$)
R_{V_p}	reaction rate per unit particle volume ($mol\ s^{-1}\ cm^{-3}$)
Re	Reynolds number
S_g	specific catalyst surface area ($cm^2\ g^{-1}$)
t	time (s)
v	velocity ($cm\ s^{-1}$)
V	volume (cm^3)
y	cartesian coordinate (cm)
z	cartesian coordinate (cm)

Greek letters

α_1	kinetic parameter ($cm^4\ mol^{-1}\ s^{-1}$)
α_2	kinetic parameter ($cm^4\ s^{-1}\ Einstein^{-1}$)
β	volumetric extinction coefficient (cm^{-1})
ε_p	porosity
η	effectiveness factor
θ	spherical coordinate (rad)
κ	volumetric absorption coefficient (cm^{-1})
λ	wavelength (nm)
μ	viscosity ($g\ cm^{-1}\ s^{-1}$)
μ	$\cos\theta$
μ_0	cosine of the angle between an incoming and a scattered ray
ρ	density ($g\ cm^{-3}$)
σ	volumetric scattering coefficient (cm^{-1})
τ^*	tortuosity
ω	σ/β = albedo

Subscripts

A	component A
att	attenuation
c	catalyst
diff	diffusion
eff	effective
ex	exit condition
ext	external
F	relative to fluid
in	inlet condition
mix	relative to the mixture
P	relative to the particle or agglomerate
R	reactor
susp	relative to suspension
S	relative to solid or superficial variable
T	total
Tk	tank
W	relative to the wall of the reactor
z	relative to z-axis
0	global
λ	relative to wavelength

Superscripts

H_R	surface at $y = H_R$
s	relative to surface
0	initial value; also surface at $y = 0$

Special symbols

$\langle\rangle$	average value over a defined space
under bar	a vector value
over bar	average value over wavelengths

an effectiveness factor of 0.9 and concluded that mass transfer limitation could be neglected. Dionysiou et al. [4] found important mass transfer limitations in a rotating disc photoreactor employing spherical particles having slightly more than 0.6 cm in diameter of titanium dioxide fixed on a solid support, and the role of mass transfer was analyzed in terms of one of the dimensionless Damköhler numbers. Mehrotra et al. [5] proposed the distinction of different working regimes in the rates of photocatalytic reactions with titanium dioxide suspensions, this work being so far one of the most complete contributions to the field. They defined an effectiveness factor for a first-order reaction, but afterwards calculated a critical radius for transport limitations (*ca.* 9 μm) employing an effectiveness factor empirically obtained taking, as a reference, the maximum observed rates for the studied reaction (benzoic acid degradation). In other

reactor configurations, particularly films and membrane reactors (with a geometry very different than the one used in this work) other quantifications of experimental observations of internal mass transfer limitations have been published (Dijkstra et al. [6], Chen et al. [7], among others). In this respect, working with membrane reactors, the outstanding work of Edwards et al. [8] is worth to be mentioned. Note that some of the above mentioned references were not dealing with slurry reactors, a circumstance that emphasizes the lack of attention that this subject has received in the scientific community. Two important and special proposals related to our work must also be mentioned. They are (i) the postulation for photochemical reactions (at that time, for homogeneous systems) of a effectiveness factor for light penetration [9] and (ii) the application of the classical effectiveness factor concept in photocatalytic reactions performed in membranes, proposed by Edwards et al. [8].

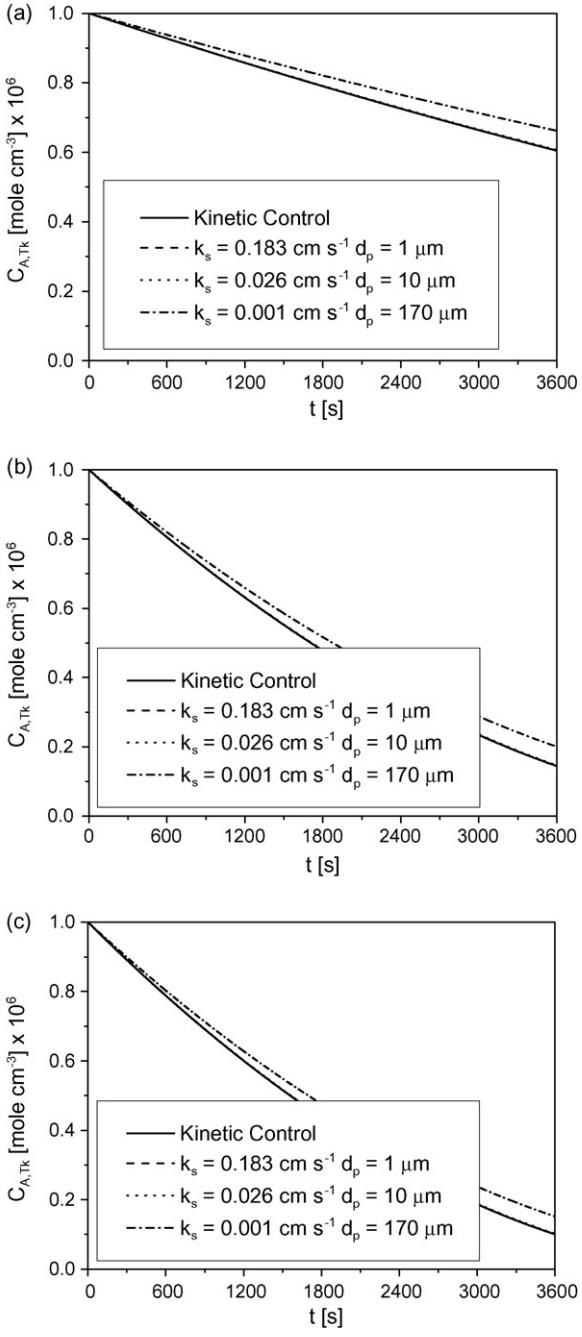

Fig. 1. External mass transfer effects as a function of changes in the mass transfer coefficient with the particle diameter at three different catalytic particle concentrations. 100% irradiation level, $R_{Het,A} \times 1$, $V_{Tk} = 3000\,cm^3$. (a) $C_{mc} = 0.1\,g\,L^{-1}$; (b) $C_{mc} = 1\,g\,L^{-1}$; (c) $C_{mc} = 3\,g\,L^{-1}$.

In our previous contribution, we constricted our analysis to the consequences on the reaction regime produced by both radiation and concentration gradients in the bulk of the reaction space. The examination of those limitations directly related to the fluid–solid interface and the interior of the solid particle (or the well-known formation of agglomerates) was left for this second work. In the interior of the particle (or agglomerate) two different phenomena must be considered: the concentration gradients and the light penetration. In this contribution, the detailed analysis of these additional phenomena will be made resorting to the fundamentals of chemical reaction engineering.

2. External solid–liquid mass transfer

In this section we will look at the problem of the possibility of external mass transfer control in the film surrounding the solid–liquid interface of the catalytic particle. Even if not absolutely necessary, to keep the continuity with the first part of this work, we will consider in our analysis the same reactor arrangement described in Fig. 1 of Ballari et al. [1]. Then, to study external transport limitations, we will consider that the flow rate is sufficiently high in the photochemical flow reactor leading to a high turbulency in the reactor ($Re > 25{,}000$) such as concentration gradients in the bulk of the reacting medium may be considered negligible. However, the second assumption does not impose the nonexistence of a resistance in the boundary layer surrounding the catalytic particle (or agglomerate) that will be conveyed with the movement of the fluid. Note that this flow condition approaching the perfect mixing behavior (PM) is achieved with a flow rate that results in a very intense turbulent flow operation. The equivalent condition in a batch reactor implies the use of a very strong mixing operation.

The most important equations for the modeling of the system will be recapitulated here. The interested reader can found the details in [1].

2.1. Basic equations

2.1.1. Mass balance

For the reactor

$$\frac{\partial C_{A,R}(y,z,t)}{\partial t} + v_{z,S}(y)\frac{\partial C_{A,R}(y,z,t)}{\partial z} - \frac{\partial}{\partial y}\left\{[D_{A,mix} + D_{A,turb}(y)]\frac{\partial C_{A,R}(y,z,t)}{\partial y}\right\} = a_V R_{Het,A,R}(y,z,t) \quad (1)$$

For the tank:

$$\frac{dC_{A,Tk,ex}(t)}{dt} = \frac{Q}{V_{Tk}}[C_{A,Tk,in}(t) - C_{A,Tk,ex}(t)] \quad (2)$$

The initial and boundary conditions for the system are

$$C_{A,R}(y, z, t = 0) = C^0_{A,R} \quad (3)$$

$$\frac{\partial C_{A,R}(y = 0, z, t)}{\partial y} = 0 \quad (4)$$

$$\frac{\partial C_{A,R}(y = H_R, z, t)}{\partial y} = 0 \quad (5)$$

To these equations one must add the logical connections between the reactor and the tank.

2.1.2. The reaction kinetics

According to Appendix A of Part I [1] a modified kinetics, needed to correct two unjustified assumptions in the work presented by Zalazar et al. [10], after recalculating the kinetic parameters from the original experimental information [11], leads to the following expression corresponding to the mechanistic scheme described in Table 2 of Part I [1]:

$$a_V R_{Het,A}(y, z, t) = S_g C_{mc} \alpha_1 C_{A,R}(y, z, t) C_{O_2} \times \left\{ 1 - \sqrt{1 + 2\frac{\alpha_2}{\alpha_1^2 S_g C_{mc} C_{A,R}(y, z, t) C_{O_2}} \int_{\lambda=275}^{\lambda=390} e^a_\lambda[(y), C_{mc}]d\lambda} \right\} \quad (6)$$

For this equation the following parameters were recalculated:

$$\alpha_1 = 2.35 \pm 0.42\ cm^4\ mol^{-1}\ s^{-1} \quad \text{and}$$
$$\alpha_2 = 1.25 \pm 0.41\ cm^4\ s^{-1}\ Einstein^{-1} \quad (7)$$

2.1.3. The radiation balance

For the case of a one-dimensional slab geometry with azimuthal symmetry, resulting from the existing diffuse emission as a consequence of the employed ground glass device (Fig. 1, in [1]), the RTE becomes [12]:

$$\mu \frac{dI_\lambda(y, \mu)}{dy} + (\kappa_\lambda + \sigma_\lambda) I_\lambda(y, \mu) = \frac{\sigma_\lambda}{2} \int_{\mu'=-1}^{\mu'=1} I_\lambda(y, \mu') p(\mu, \mu')\ d\mu' \quad (8)$$

The diffuse and isotropic inlet boundary conditions are:

$$I_\lambda(y = 0, \mu) = I^0_\lambda \quad \text{for} \quad \mu > 0 \quad (9)$$

$$I_\lambda(y = H_R, \mu) = I^{H_R}_\lambda \quad \text{for} \quad \mu < 0 \quad (10)$$

The employed phase function is:

$$p_{HG,\lambda}(\mu_0) = \frac{1 - g^2_\lambda}{(1 + g^2_\lambda - 2g_\lambda \mu_0)^{3/2}} \quad (11)$$

The adopted value of the total incident radiation ($275\ nm \le \lambda \le 390\ nm$) from each side of the reactor and without filters, measured with potassium ferrioxalate actinometry [13] was: $G_W = 1.84 \times 10^{-6}$ Einstein $cm^{-2}\ s^{-1}$. The values of the dimensionless asymmetry factor g_λ and other optical properties of the adopted catalyst are given in Table 3 of Part 1 [1].

Solution of Eqs. (8)–(11) was numerically obtained with the discrete ordinate method [14]. From the values of specific intensities the local volumetric rate of photon absorption (LVRPA) results:

$$e^a_\lambda[(y), C_{mc}] = \kappa_\lambda \left\{ 2\pi \int_{\mu=-1}^{1} I_\lambda[(y, \mu), C_{mc}]d\mu \right\} \quad (12)$$

2.2. Modeling the external mass transfer control

Combining the reaction rate with the mass transfer rate in the external film surrounding the catalytic particle, and using a volumetric mass transfer rate we obtain [15]:

$$a_V R_{Het,A} = k_S a_V (C^s_A - C_A) \quad (13)$$

Extracting C^s_A from Eq. (13), substituting into Eq. (6) and after some grouping according to Appendix A:

$$a_V R_{Het,A} = \frac{((m/k_S a_V) + nC_A) - [((m/k_S a_V) + nC_A)^2 + 4mC_A(1 - (n/k_S a_V))]^{1/2}}{2(1 - (n/k_S a_V))} \quad (14)$$

The value of k_s can be obtained from the empirical correlation of Calderbank and Moo-Young [16] for small particles:

$$\frac{k_S d_P}{D_{A,mix}} = 2.0 + 0.31 \left[\frac{d^3_P(\rho_P - \rho_F)g}{\mu D_{A,mix}} \right]^{1/3} \quad (15)$$

Results for different particle diameters and the values of the employed properties are shown in Table 1. The often reported catalyst agglomeration has been taken into account.

Fig. 1(a)–(c) shows the results for three different catalyst concentrations: $0.1 \times 10^{-3}\ g\ cm^{-3}$, $1 \times 10^{-3}\ g\ cm^{-3}$ and $3 \times 10^{-3}\ g\ cm^{-3}$. The solid line assumes that $k_s \to \infty$. It can be seen that only for very large catalyst particle agglomeration sizes (170 μm in the plot), almost never reported for pure titanium dioxide in suspensions, some sort of external mass transfer control can be observed. For all other particle agglomeration sizes the concentration profile coincides with the case of negligible external solid–liquid transfer. For a particle agglomeration

Table 1
Mass transfer coefficient for different catalyst particle size

Particle size, d_p (μm)	Mass transfer coefficient, k_s ($cm\ s^{-1}$)
0.2	0.879
1	0.183
5	0.043
10	0.026
170	0.001

$D_{A,mix} = 8.7 \times 10^{-6}\ cm^2\ s^{-1}$, $\rho_P = 3.84\ g\ cm^{-3}$, $\rho_F = 1\ g\ cm^{-3}$, $\mu = 1.0019 \times 10^{-2}\ g\ cm^{-1}\ s^{-1}$, and $g = 980\ cm\ s^{-2}$.

sizes of 1–10 μm often used [3,17] we will have a look at the effect produced by the assumption that the employed catalyst is 10 and 30 times more active. This can be done assuming with a virtual change that, employing a different catalyst (all other properties remaining invariable), the recombination rate of electrons and holes experiments a large reduction, affecting the value of the rate constants α_1 and α_2. Fig. 2(a)–(c) shows the results for the three cases, the last two with the rate artificially increased by modifying the value of α_1 and α_2. It can be seen

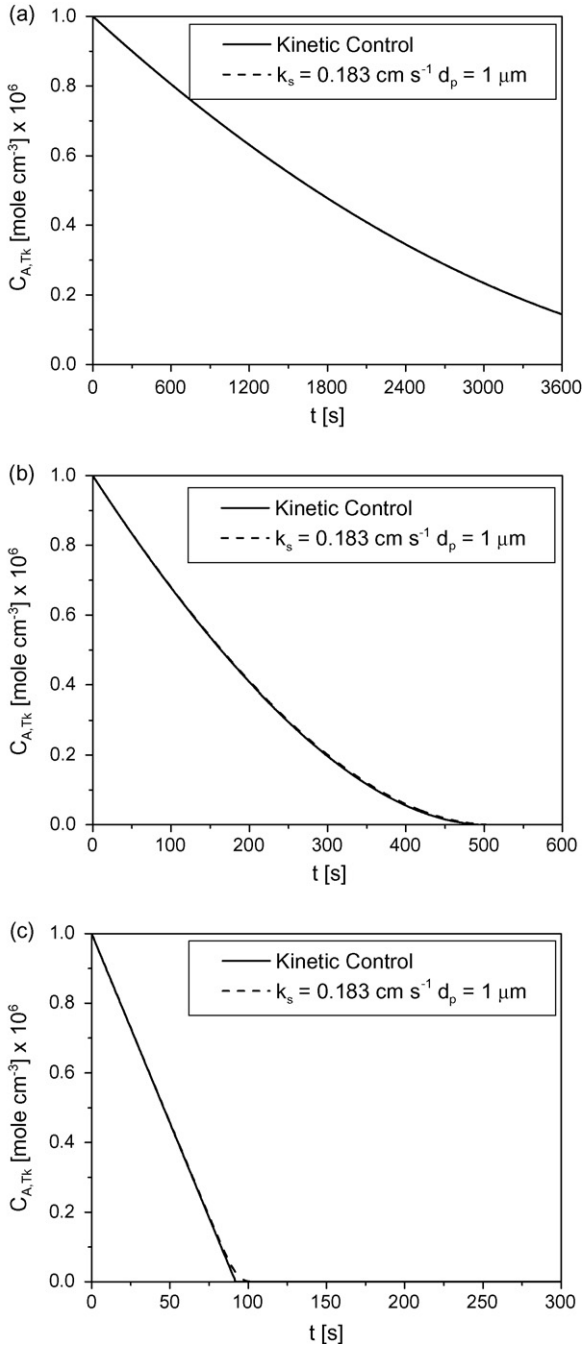

Fig. 2. Influence of the reaction rate value on the external mass transfer control, imposing a virtual change on the electron-hole recombination rate. $C_{mc} = 1\,g\,L^{-1}$, 100% irradiation level, $V_{Tk} = 3000\,cm^3$. (a) $R_{Het,A} \times 1$; (b) $R_{Het,A} \times 10$; (c) $R_{Het,A} \times 30$.

that only for a reaction rate 30 times larger, there is a very slight difference with respect to the case of $k_s \to \infty$. One can infer, from this point of view that in realistic slurry photocatalytic reactors employing the most common varieties of pure titanium dioxide, external mass transfer limitations can be safely neglected.

There is a second variable described before in Eq. (6) that can change the kinetics and give rise to mass transfer control. It is the existence of strong irradiation rates. In these cases the reaction rate on the particle surface may be so high that the concentration of the reacting species may be strongly depleted. Fig. 3(a)–(c) shows the results. Increasing the irradiation rate 100% (above the nominal pivoting value employed in this work), slight changes can be observed only when, at the same time, the reaction rate is modified by a factor of 10 or 30. Similar results are obtained when the initial DCA concentration is reduced one order of magnitude [Fig. 4(a)–(c)] even though the driving force is dramatically reduced. Only for very large particle agglomerations a deviation can be recognized.

We may conclude that under conditions of very intense macroscopic mixing, external mass transfer limitations in the boundary layer surrounding the catalyst agglomerate can only be present for particle sizes above 150 μm. It is interesting to note that, the work reported by Sclafani et al. [2] was performed in a packed bed reactor, and consequently their results are not useful to confirm our conclusion. Although they were employing particles having a relatively large diameter, it must be clear that the reactor configuration reported in Ref. [2] does not belong to the type of problems studied in this work. Titanium dioxide immobilized in different supports and used in packed beds, catalytic walls or membranes reactors, require an analysis performed in different terms because Eqs. (1)–(12) and (14) are only valid for slurry reactors. Consequently, the conclusion drawn before does not apply to these different families of photocatalytic reactors. An additional comment is necessary. When titanium dioxide is supported on particles of larger size (silica, activated charcoal, etc.) in order to improve pollutant absorption rates or to avoid downstream catalyst separation costs ([18], for example), this type of mass transfer limitation may be present and will have to be taken into account. However, it is fair to recognize that supported titanium dioxide in particles of larger size are just beginning to be used in slurry reactors, the reference cited above being one of these exceptions.

3. Internal particle mass transfer limitations

This is a problem that has two different components that should be decoupled: (i) the diffusion of reactants and products in and out of the interior of the particle and (ii) the light penetration inside the catalyst volume. The first consideration that must be taken into account is that working with pure titanium dioxide most of the available catalyst are non-porous (e.g., Degussa P 25, Hombikat 100, Aldrich, etc.) and the so called porosity is mainly the result of catalyst agglomeration that is a strong function of the working pH [19]. Agglomeration sizes have been observed with light scattering and electron microscopy

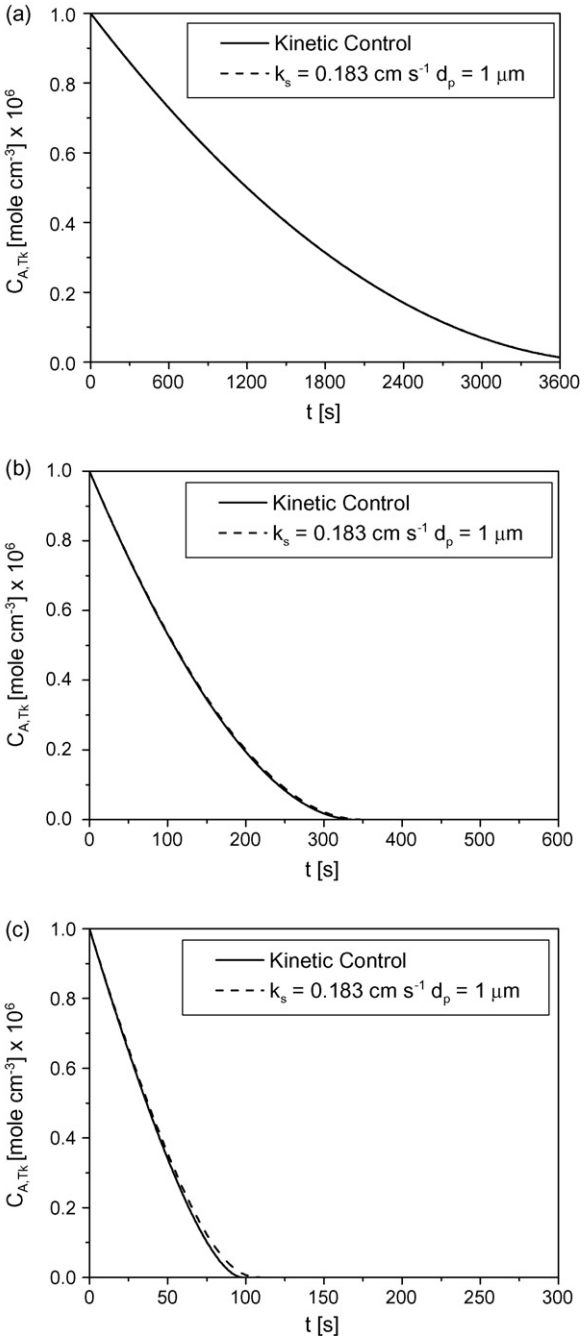

Fig. 3. Influence of the reaction rate value on the external mass transfer control, imposing a virtual change on the electron-hole recombination rate and a virtual increase in the irradiation rate. $C_{mc} = 1\,g\,L^{-1}$, 200% irradiation level, $V_{Tk} = 3000\,cm^3$. (a) $R_{Het,A} \times 1$; (b) $R_{Het,A} \times 10$; (c) $R_{Het,A} \times 30$.

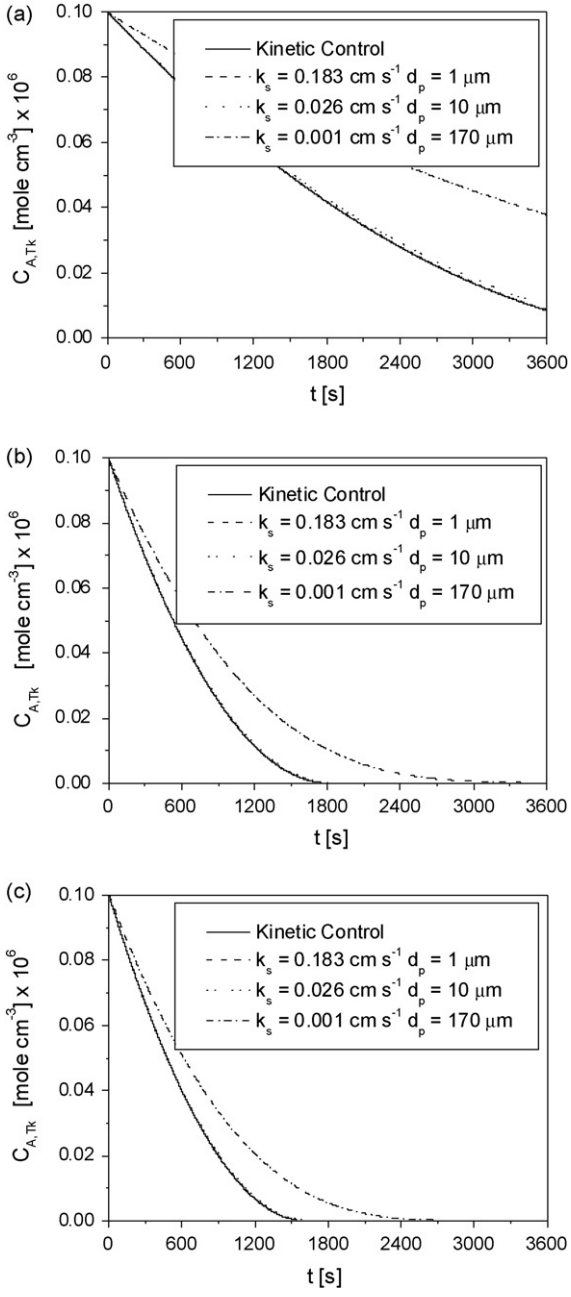

Fig. 4. Influence of the initial pollutant concentration that has been changed one order of magnitude (from 1×10^{-6} to 1×10^{-7} mol cm^{-3}), on the external mass transfer control. 100% irradiation level, $R_{Het,A} \times 1$, $V_{Tk} = 3000\,cm^3$; (a) $C_{mc} = 0.1\,g\,L^{-1}$: (b) $C_{mc} = 1\,g\,L^{-1}$; (c) $C_{mc} = 3\,g\,L^{-1}$.

techniques [17,19], with sized ranging from *ca.* 1 μm to values sometimes as large as 10 μm or more. The degree of agglomeration directly defines the porosity of the employed catalyst.

3.1. The effectiveness factor

The concept of catalyst effectiveness in homogeneous photochemical reactions was put forward for the first time by Camera Roda and Santarelli [9]. The problem in heterogeneous reactors is certainly more complex but the extension of the original idea is a very suitable tool for analyzing the photocatalytic particle internal limitations.

Let us define the overall effectiveness:

$$\eta_0 = \frac{\langle R_{V_P,A}[C_A(r), e_S^a(r)]\rangle_{V_P}}{R_{V_P,A}[C_A^s(R_P), e_S^a(R_P)]} \tag{16}$$

Eq. (16) can be written as:

$$\eta_0 = \underbrace{\frac{\langle R_{V_P,A}[C_A(r), e^a_S(r)]\rangle_{V_P}}{\langle R_{V_P,A}[C^s_A(R_P), e^a_S(r)]\rangle_{V_P}}}_{\eta_{diff}\text{ (diffusive mass transfer effectiveness factor)}} \times \underbrace{\frac{\langle R_{V_P,A}[C^s_A(R_P), e^a_S(r)]\rangle_{V_P}}{R_{V_P,A}[C^s_A(R_P), e^a_S(R_P)]}}_{\eta_{att}\text{ (photon transport effectivenes factor)}} \quad (17)$$

Such as:

$$\eta_0 = \eta_{diff} \times \eta_{att} \quad (18)$$

The first factor represents the reaction rate in the particle taking place with the rate of electron-hole generation calculated as a function of the radiation distribution inside the particle, divided by the same reaction rate calculated with the pollutant concentration at the external surface of the particle, but maintaining the radial distribution of the local superficial rate of photon absorption inside the particle. The numerator of the second factor includes all the limitations produced by the light penetration restrictions, considering that there are no limitations to the penetration of reactants (or exit of reaction products) inside the catalytic particle. The interpretation of the denominator of the second factor is trivial.

The analysis of the problem requires the following steps: (1) to obtain a kinetic expression per unit particle volume instead of a pseudo-homogeneous expression for the elementary suspension volume; (2) to uncouple the mass transfer problem from the radiation transport problem that are combined in the kinetic equation; (3) to solve the mass transfer equation for the particle (agglomerate) assuming that there are no photons transport limitations; (4) to solve the photon transport inside the particle without chemical reaction; (5) to combine both results at the interior of the particle, in a superficial reaction including both limitations. The following variables will be explored: (i) wavelength, due to its effects on the optical properties of the catalyst, (ii) superficial concentration of DCA, (iii) catalyst porosity and (iv) agglomeration diameter.

To show in a clear manner the particular effect produce by the wavelength of the employed radiation, we will work with two hypothetically reactors operating with monochromatic light at 305 nm (the region under exploration having high emission by the lamp and high radiation absorption by the catalyst) and 370 nm (a region of high emission by the mercury lamp but low absorption by titanium dioxide). Other parameters are described in Table 2.

Table 2
Employed parameters for internal mass and photon transfer limitations

Denomination and/or definition	Values	Units
DCA concentration in the bulk (C_A)[a]	1×10^{-6} to 1×10^{-10}	mol cm^{-3}
Catalyst concentration (C_{mc})	(0.5 and 3) $\times 10^{-3}$	g cm^{-3}
Agglomerate porosity (ε_P)	0.3–0.5	
Agglomerate size (d_p)	1–40	μm
Wavelength	305 and 370	nm
Incident radiation[b]	(0.8 and 2.6) $\times 10^{-7}$	Einstein cm^{-2} s^{-1}
Absorption coefficient[c]	1.5×10^5 (305 nm) 0.4×10^5 (370 nm)	cm^{-1}
Albedo [($\omega_P=\sigma_P/\beta_P$); ($\beta_P=\kappa_P+\sigma_P$)]	0 and 0.73	

[a] Calculated at $z=0$ and at the initial conditions ($t=0$), even though the value of 1×10^{-10} mol cm^{-3} has been thought as a concentration corresponding to the end of a run.
[b] Calculated at $y=0+\delta$ or $y=H_R-\delta$ with $\delta\to0$.
[c] Data calculated from information taken from [20] at the wavelengths under study.

3.2. Kinetic equation per unit particle volume

From Eq. (6) we have:

$$R_{V_P,A} = a_{V_P} R_{Het,A} = \frac{a_{V_P}}{a_V} S_g C_{mc} \alpha_1 C_A C_{O_2} \times \left\{1 - \sqrt{1 + 2\frac{\alpha_2}{\alpha_1^2 S_g C_{mc} C_A C_{O_2}} \int_{\lambda=275}^{\lambda=390} e^a_\lambda[(y), C_{mc}]d\lambda}\right\} \quad (19)$$

where:

$$a_{V_P} = \frac{A_{F-S}}{V_P} = S_g \rho_p = S_g \rho_S (1-\varepsilon_P) \quad (20)$$

With the proper transformations and some algebra, Eq. (19) is equivalent to:

$$R_{V_P,A} = a_{V_P} R_{Het,A} = S_g \rho_P \alpha_1 C_A C_{O_2} \times \left\{1 - \sqrt{1+2\frac{\alpha_2}{\alpha_1^2 C_A C_{O_2}} \int_{\lambda=275}^{\lambda=390} e^a_{S,\lambda}[(y), C_{mc}]d\lambda}\right\} \quad (21)$$

3.3. The particle mass balance

The mass balance is:

$$-\underline{\nabla}\cdot(D_{A,eff}\underline{\nabla}\langle C_A\rangle) = -a_{V_P} R_{Het,A} \quad (22)$$

Let as assume a spherical geometry and consider that there is symmetry in the θ and ϕ directions (Fig. 5). Assuming further that the effective diffusivity is uniform:

$$-\frac{D_{A,eff}}{r^2}\frac{d}{dr}\left[r^2\frac{dC_A(r)}{dr}\right] = -a_{V_P} R_{Het,A}(r) \quad (23)$$

With the boundary conditions:

$$r=0 \to \frac{dC_A}{dr} = 0 \quad \text{and} \quad r=R_P \to C_A = C^s_A \quad (24)$$

And the classical definition:

$$D_{A,eff} = \frac{D_{A,mix}\varepsilon_P}{\tau^*} \quad (25)$$

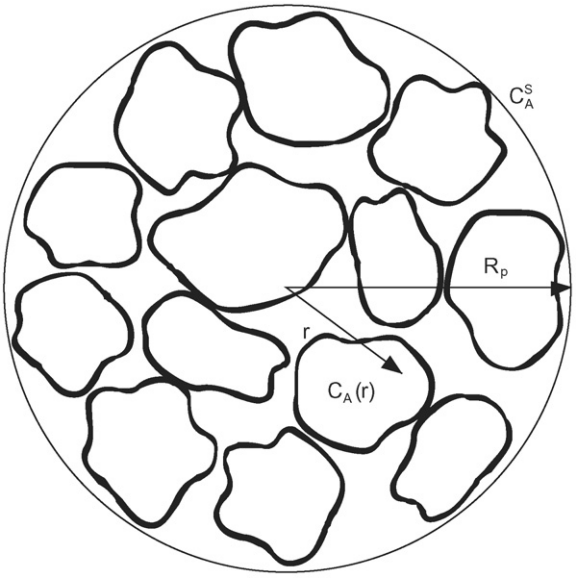

Fig. 5. Schematic representation of an agglomerate.

The averaged rate per particles is:

$$\langle R_{V_P,A}\rangle_{V_P} = \frac{4\pi}{V_P}\int_0^{R_P} R_{V_P,A}(r)r^2\,dr \tag{26}$$

Solving these equations, it is not yet possible to calculate the numerator of the first factor in Eq. (17) because we do not know de distribution of e_S^a as a function of the radius. Even if there are no external mass transfer restrictions, the denominator has still the same problem. This critical aspect will be analyzed in the next section. In both cases, a decision must be made concerning the point inside the reactor volume where $C_A^s(y, z, t)$ and the radiation boundary condition (to calculate e_S^a as a function of the y-position) is selected. The choice was to use points very close to $y = 0$ or $y = H_R$, $z = 0$ (reactor inlet) and $t = 0$ (initial conditions). The explanation of these adoptions (with the exception of the one concerning $t = 0$) are clearly deduced from the results depicted in Fig. 6(a) and (b) obtained from the solution of Eqs. (8)–(12). More information is given in Table 2. Clearly, we have adopted the most critical condition inside the reactor space.

3.4. The photon absorption distribution inside the particle

The radiation field inside the particle must be modeled in order to know the radiation profiles as a function of the distance from the particle (agglomerate) surface to its center. A variation of the two flux model, called the Eddington approximation will be used [21,22]. The detailed derivation to reach a differential equation for the incident radiation is given in Appendix B. The result in spherical coordinates is:

$$\frac{1}{r^2}\frac{d}{dr}\left(r^2\frac{dG_P}{dr}\right) = 3(1-\omega_P)\beta_P^2 G_P \tag{27}$$

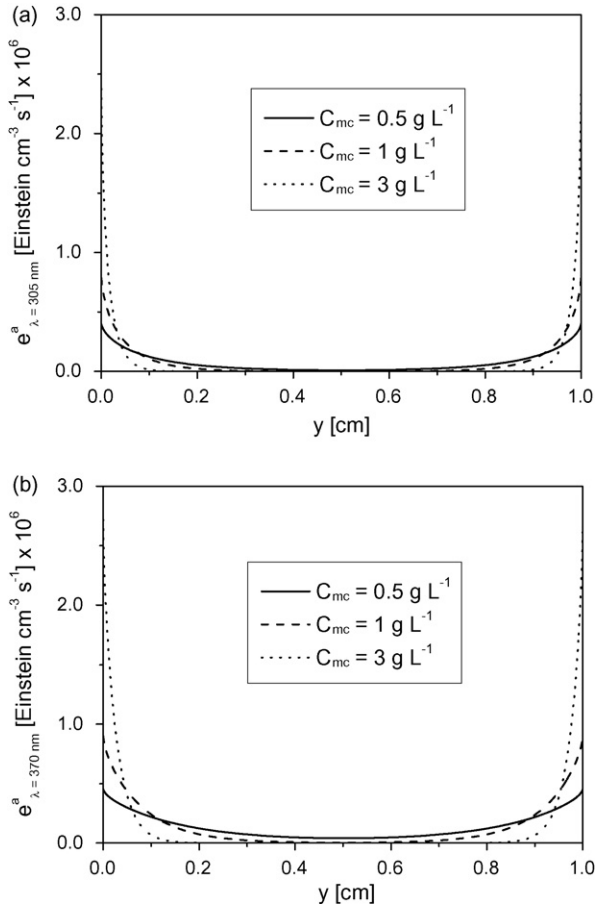

Fig. 6. LVRPA distribution in the reactor space as a function of the reactor thickness. (a) For $\lambda = 305$ nm; (b) For $\lambda = 370$ nm. Data are used to decide the point inside the reactor where internal mass and photon transport limitations will be analyzed.

With the following boundary conditions:

$$\begin{aligned} &r = R_P \rightarrow G_P = G_P(R_P)\\ &r = 0 \rightarrow \frac{dG_P}{dr} = 0 \end{aligned} \tag{28}$$

Let us call $3(1-\omega_P)\beta_P^2 = \gamma^2$. The solution of Eq. (27) after application of the B. Cs. is:

$$G_P(r) = G_P(R_P)\left(\frac{R_P}{r}\right)\frac{\sinh(\gamma r)}{\sinh(\gamma R_P)} \tag{29}$$

and:

$$q_{r,P}(r) = -\frac{G_P(r)\gamma}{3\beta_P}\left[\frac{1}{\tanh(\gamma r)} - \frac{1}{\gamma r}\right] \tag{30}$$

The net radiation flux at the surface of the particle, results:

$$q_{r,P}(R_P) = -G_P(R_P)\frac{\gamma}{3\beta_P}\left[\frac{1}{\tanh(\gamma R_P)} - \frac{1}{\gamma R_P}\right] \tag{31}$$

As shown in Appendix C, Eq. (31) has a noticeable similitude with the mass transfer effectiveness factor in spherical catalytic pellets.

The problem at this point is that we do not have an expression for the value of $G_P(R_P)$. In order to look for a solution to

this limitation we must relate the radiation arriving to the particle from the suspension (the external field) to that effectively absorbed in the particle volume. This can be done performing a radiation flux balance on the surface of the agglomerate. As shown in Appendix D:

$$G_P(R_P) = \frac{\rho_P}{C_{mc}} \frac{R_P \beta_P}{\gamma} e^a_{susp} \frac{1}{[(1/\tanh(\gamma R_P)) - (1/\gamma R_P)]} \quad (32)$$

Using the solution provided by Eq. (29):

$$e^a_P(r) = \kappa_P G_P(r) = \kappa_P G_P(R_P) \frac{R_P}{r} \frac{\sinh(\gamma r)}{\sinh(\gamma R_P)} \quad (33)$$

Substituting Eq. (32):

$$e^a_P(r) = \frac{\rho_P}{C_{mc}} e^a_{susp} \frac{R_P}{r} \frac{\sinh(\gamma r)}{\sinh(\gamma R_P)} \times \frac{1}{(3/\gamma R_P)[(1/\tanh(\gamma R_P)) - (1/\gamma R_P)]} \quad (34)$$

Defining the LSRPA inside the particle:

$$e^a_S(r) = \frac{e^a_P(r)}{a_{V_P}} = \frac{e^a_P(r)}{S_g \rho_P} \quad (35)$$

Combining Eqs. (34) and (35) we finally obtain:

$$e^a_S(r) = \frac{e^a_{susp}}{S_g C_{mc}} \frac{R_P}{r} \frac{\sinh(\gamma r)}{\sinh(\gamma R_P)} \times \frac{1}{(3/\gamma R_P)[(1/\tanh(\gamma R_P)) - (1/\gamma R_P)]} \quad (36)$$

Eq. (36) relates the value of the LVRPA that can be obtained from the solution of the RTE in the suspension (indicated for clarity with the subscript "susp") to the existing LSRPA when all the external surface of the particle is available, i.e., for $r = R_P$. From previous results in Part I [1] we know the value of $e^a_{susp,\lambda}(y)$ as a function of position and, consequently, it allows us to calculate e^a_S.

At this point, we can recover, for consistency, the subscript λ to recall that we are using monochromatic light. Note that if we were working with polychromatic radiation:

$$e^a_{S,\sum\lambda} = \sum_{\lambda=\lambda_1}^{\lambda=\lambda_n} e^a_{S,\lambda}(r, y). \quad (37)$$

3.5. The diffusive effectiveness factor

With Eq. (36) now we have all the elements to calculate the diffusive effectiveness factor. The obtained values for η_{diff} are reported in Tables 3 and 4. Under most of the chosen operating conditions, the value of η_{diff} does not shows very significant changes unless the pollutant concentration becomes very low and the catalyst radiation absorption coefficient is also very low. This can be seen, for example, in the case when $C^s_A(y \approx 0,\ z = 0,\ t = 0) = 1$ ppm and $\lambda = 370$ nm. This clearly means that when the catalyst absorption coefficient is small and the reactant concentration is equally small (indicating a lower reaction rate), the driving force in the mass transport process is much more intensively reduced and diffusion limitations become, to some extent, more important. At 305 nm, changes are not very significant but as expected, when the porosity decreases and the particle size increases, some small reductions in the diffusive efficiency are observed. Not very important sensitivity can be perceived with the change in the catalyst loading. With the same trend, at 370 nm, results are barely more evident with the exception quoted above for low C^s_A concentrations. These results are clearly shown in Fig. 7(a)–(c). Results in Fig. 7(a), shown

Table 3
Effectiveness factors at 305 nm ($\kappa_P = 1.5 \times 10^5$ cm^{-1} and $\omega_P = 0$)

C_A ($\times 10^8$ mol cm^{-3})	C_{mc} ($\times 10^3$ g cm^{-3})	ε_P	e^a ($\times 10^7$ Einstein cm^{-3} s^{-1})	R_P (μm)	η_{diff}	η_{att}	η_0
100	0.5	0.3	4	1	0.9996	0.2741	0.2740
100	0.5	0.3	4	5	0.9990	0.0629	0.0628
100	0.5	0.3	4	10	0.9986	0.0322	0.0321
100	0.5	0.3	4	20	0.9981	0.0166	0.0166
100	3	0.3	25	1	0.9996	0.2742	0.2741
100	3	0.3	25	5	0.9990	0.0629	0.0628
100	3	0.3	25	10	0.9986	0.0322	0.0321
100	3	0.3	25	20	0.9981	0.0166	0.0166
100	3	0.4	25	1	0.9997	0.3111	0.3110
100	3	0.4	25	5	0.9992	0.0729	0.0728
100	3	0.4	25	10	0.9988	0.0374	0.0373
100	3	0.4	25	20	0.9984	0.0192	0.0192
1	0.5	0.3	4	1	0.9962	0.2762	0.2751
1	0.5	0.3	4	5	0.9899	0.0633	0.0626
1	0.5	0.3	4	10	0.9858	0.0324	0.0319
1	0.5	0.3	4	20	0.9811	0.0167	0.0164
1	3	0.3	25	1	0.9961	0.2762	0.2751
1	3	0.3	25	5	0.9897	0.0633	0.0626
1	3	0.3	25	10	0.9855	0.0324	0.0319
1	3	0.3	25	20	0.9807	0.0167	0.0164

Table 4
Effectiveness factors at 370 nm ($\kappa_P = 4 \times 10^4\ cm^{-1}$, $\omega_P = 0.73$)

C_A ($\times 10^8$ mol cm^{-3})	C_{mc} ($\times 10^3$ g cm^{-3})	ε_P	e^a ($\times 10^7$ Einstein cm^{-3} s^{-1})	R_P (μm)	η_{diff}	η_{att}	η_0
100	0.5	0.3	4	1	0.9992	0.4566	0.4562
100	0.5	0.3	4	5	0.9974	0.1184	0.1181
100	0.5	0.3	4	10	0.9962	0.0613	0.0611
100	0.5	0.3	4	20	0.9946	0.0314	0.0312
100	3	0.3	25	1	0.9992	0.4566	0.4562
100	3	0.3	25	5	0.9974	0.1184	0.1181
100	3	0.3	25	10	0.9961	0.0613	0.0611
100	3	0.3	25	20	0.9945	0.0314	0.0312
100	3	0.4	25	1	0.9994	0.5055	0.5052
100	3	0.4	25	5	0.9979	0.1366	0.1363
100	3	0.4	25	10	0.9969	0.0711	0.0709
100	3	0.4	25	20	0.9955	0.0364	0.0363
1	0.5	0.3	4	1	0.9918	0.4588	0.4550
1	0.5	0.3	4	5	0.9738	0.1193	0.1162
1	0.5	0.3	4	10	0.9620	0.0617	0.0594
1	0.5	0.3	4	20	0.9468	0.0316	0.0299
1	3	0.3	25	1	0.9917	0.4588	0.4550
1	3	0.3	25	5	0.9733	0.1193	0.1161
1	3	0.3	25	10	0.9612	0.0617	0.0593
1	3	0.3	25	20	0.9457	0.0316	0.0298

for $\lambda = 370$ nm, have the pollutant concentration as a parameter whereas Fig. 7(b) employed as a parameter the two adopted wavelengths for this study. In both cases the plot represents the diffusive effectiveness factor as a function of the particle (agglomerate) radius, including as an anticipation, results for the photon transport effectiveness factor. Also, in Fig. 7(c) it can be observed the influence on the results when the particle radius (agglomerate) changes from 1 μm to 20 μm, producing an important change in the diffusive effectiveness factor. It is also noted in this representation, that the concentration of the pollutant (C_A^s) affects the diffusive effectiveness factor more significantly when the particle (agglomerate) radius is increased which is in accordance with the classical definition of the effectiveness factor. It should be noted that when the radiation absorption decreases, the reaction rate also decreases, but the averaged value of the reaction rate becomes larger and consequently the efficiency decreases. In effect, if the radiation absorption coefficient decreases one should expect a higher effectiveness factor (close to 1) because the reaction kinetics is low and the system should operate under the kinetic control regime. The results in Fig. 7(b) indicate the opposite behavior because the effectiveness factor is lower for a wavelength where radiation absorption by the catalyst is low. This is the result of the following effect: the average reaction rate is higher for the case of low radiation absorption because radiation reaches almost all the available catalytic surface, i.e., it can even reach the centre of the particle. Conversely for the case in which radiation absorption is very high (at lower wavelengths) there is a very high reaction rate on the catalytic external surface but a much reduced value in the rest of the available area inside the particle, because almost no radiation arrives there to activate the catalysts. This effect produces a smaller average reaction rate per particle, favouring the kinetic control.

3.6. The attenuation effectiveness factor

Once more Eq. (36) must be used to calculate the numerator of the second factor of Eq. (17). The denominator results from substituting r for R_P in the same equation. Then, the attenuation effectiveness factor can be calculated. Tables 3 and 4 show the results of the values corresponding to η_{att} and η_0. It is quite clear that the limitations are almost always due to the light penetration on account of the very strong radiation absorption properties of titanium dioxide. A very important conclusion previously noted during the discussion of the diffusive effectiveness factor is that a process that starts at relatively large concentration of the pollutant, during the course of the reaction, in some cases, can switch from the kinetic control regime to the one of mass transfer limitations when the concentration of the chemical compound reaches very small values and this is noted in the value of the overall efficiency (η_0). This eventual change in the reaction performance is particularly important in kinetic studies.

Regarding the results concerning η_{att} it must be taken into account that the penetration of radiation in the agglomerate depends on the wavelength that define the properties of the catalyst and the porosity, and is independent of the agglomerate radius. The observed, sometimes very drastic, changes in the portrayed results [Fig. 7(a)–(c)] are due to the relative values of the radiation penetration depth with respect to the particle radius, which are directly translated into the average reaction rate per particle volume calculated with Eq. (26). This observation has a very simple explanation: the penetration depth depends on the above mentioned variables, but once they have been taken into account, a further increase in the size of the particle cannot affect the light penetration any longer and the light activation cannot progress any further. It should also be noted that the attenuation efficiency is independent of the DCA concentra-

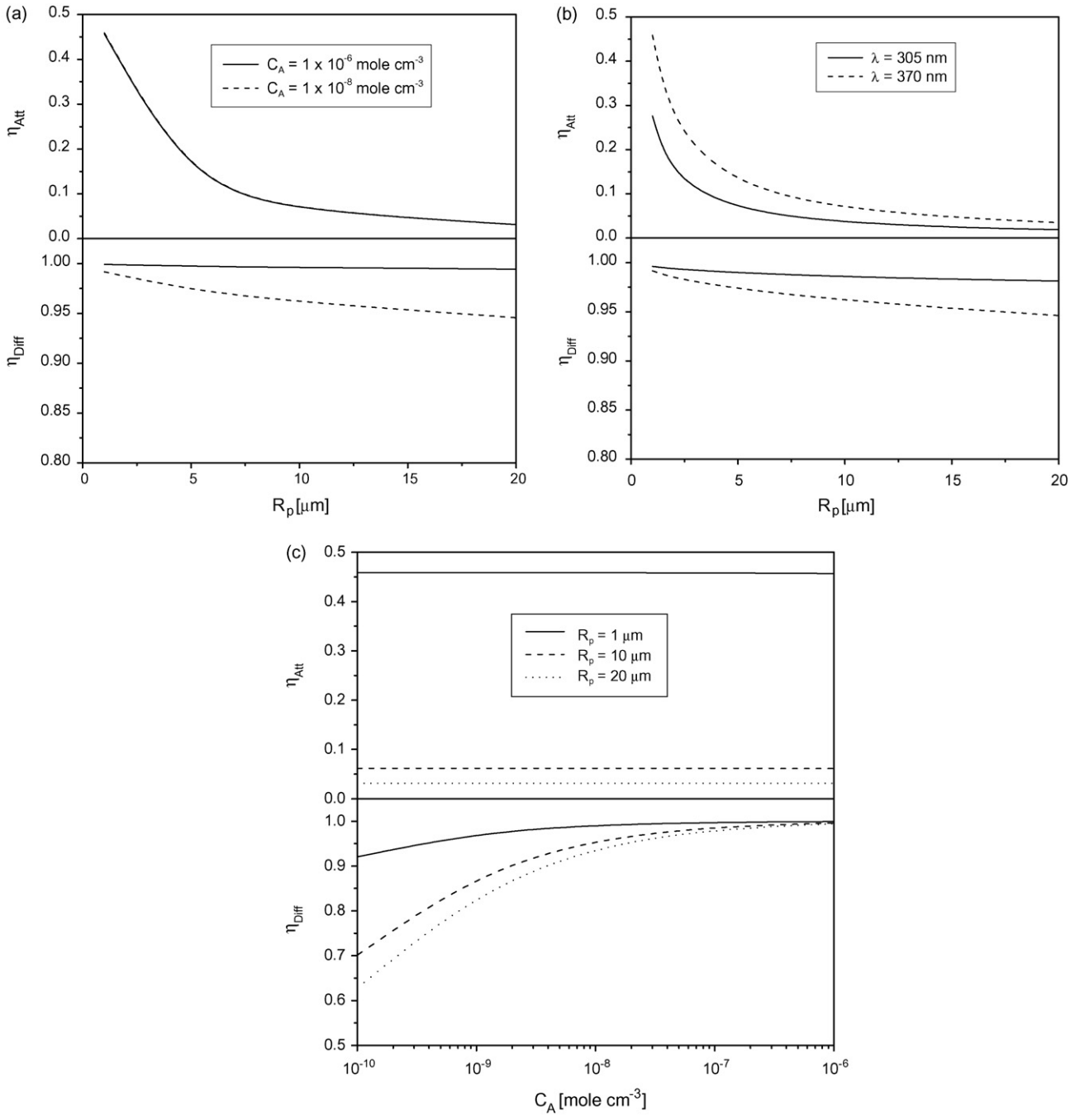

Fig. 7. Effectiveness factors. (a) Effect of the particle (agglomerate) radius. C_A is the parameter; $\lambda = 370$ nm, $C_{mc} = 3\ g\ L^{-1}$, $\kappa_P = 40{,}000\ cm^{-1}$, $\omega_P = 0.73$, $\varepsilon_P = 0.3$, $e^a = 2.5 \times 10^{-6}$ Einstein $cm^{-3}\ s^{-1}$. (b) Effect of the particle (agglomerate) radius. The employed wavelength is the parameter $C_A = 1 \times 10^{-8}$ mol cm^{-3}, $C_{mc} = 3\ g\ L^{-1}$, $\varepsilon_P = 0.3$, $e^a = 2.5 \times 10^{-6}$ Einstein $cm^{-3}\ s^{-1}$. (c) Effect of C_A. Particle radius is the parameter. $\lambda = 370$ nm, $C_{mc} = 3\ g\ L^{-1}$, $\kappa_P = 40{,}000\ cm^{-1}$, $\omega_P = 0.73$, $\varepsilon_P = 0.3$, $e^a = 2.5 \times 10^{-6}$ Einstein $cm^{-3}\ s^{-1}$.

tion. In Fig. 7(a) the solid line also includes (superimposed) the dotted line. This is nothing more than the effect produced by the previously indicated transparency of DCA to the employed radiation.

4. Conclusions

The possibility of external and internal mass transport limitations in photocatalytic suspensions of pure titanium dioxide have been analyzed in a detailed study based on fundamental principles and a realistic kinetics derived from a complete reaction mechanisms. The most important conclusions concerning mass transfer limitation in the catalytic particle or its agglomerates are:

1. External, interfacial mass transport in the boundary layer surrounding the catalytic particle, could be observed only for rather large particle sizes, not usually employed in suspensions of pure titanium dioxide.

2. Internal mass transfer limitations in catalyst agglomerates will almost always be present but, with a few exceptions (at very low reactant concentrations), they are mostly produced by light penetration restrictions (described by the attenuation effectiveness factor). This effect results from the very strong radiation absorption characteristics of titanium dioxide. Due to this circumstance, even for particle sizes (agglomerates) below 1 μm the reaction rate will not be under the kinetic control regime.
3. Mass transfer limitations inside the catalytic particle, described by the diffusive effectiveness factor are of lesser significance.

Acknowledgements

Thanks are given to Universidad Nacional del Litoral, CONICET and Agencia Nacional de Promoción Científica y Tecnológica for financial help and the doctoral fellowship of M.M.B. The technical assistance of Eng. Claudia Romani is gratefully appreciated.

Appendix A

Combining Eqs. (6) and (13):

$$a_V R_{Het,A} = S_g C_{mc} \alpha_1 \left(\frac{R_{Het,A} a_V}{k_S a_V} + C_A \right) C_{O_2} \times \left\{ 1 - \sqrt{1 + 2 \frac{\alpha_2}{\alpha_1^2 S_g C_{mc} ((R_{Het,A} a_V / k_S a_V) + C_A) C_{O_2}} \int_{\lambda=275}^{\lambda=390} e_\lambda^a [(y), C_{mc}] d\lambda} \right\} \quad \text{(AI.1)}$$

With:

$$a_V = \frac{A_{F-S}}{V_{susp}} = S_g C_{mc} \quad \text{(AI.2)}$$

To simplify notation, let us define:

$$m = 2\alpha_2 S_g C_{mc} C_{O_2} \int_{\lambda=275}^{\lambda=390} e_\lambda^a [(y), C_{mc}] d\lambda,$$
$$n = 2\alpha_1 S_g C_{mc} C_{O_2} \quad \text{(AI.3)}$$

Considering Eq. (AI.1) and solving for $a_V R_{Het,A}$, Eq. (14) in the main text of this work is obtained.

Appendix B

The Eddington approximation offers an analytic solution that is appropriated for this reaction engineering problem. The following procedure may be followed: we write the radiative transfer equation in a one-dimensional (r)–one-directional ($\mu = \cos\theta$) representation of the radiation field and calculate the zero- and first-order moments of the direction of radiation propagation: ($2\pi \int_\mu d\mu$) and ($2\pi \int_\mu \mu\, d\mu$). The results are:

$$\underline{\nabla} \cdot \underline{q_P}(r) = -(1 - \omega_P) \beta_P G_P(r) \quad \text{(AII.1)}$$

$$c[\underline{\nabla} P_P(r)]_r = -\beta_P q_{r,P}(r) \quad \text{(AII.2)}$$

Here, $q_{r,p}(r)$ is the net radiation flux, $G_p(r)$ the incident radiation, c the speed of the light and $P_p(r)$ is the radiation pressure. All possible directions are then divided in two parts: (1) forwardly directed rays ($0 \le \mu \le 1$) and (2) backwardly directed rays ($-1 \le \mu \le 0$) which permits to define forward and backward intensities $\{[I^+(r, \mu)$ and $I^-(r, \mu)]\}$. The Eddington approximation assumes that the intensities are not a function of μ to calculate $G_p(r)$, $q_{r,p}(r)$ and $P_p(r)$. Then:

$$G_P(r) = 2\pi \{[I^+(r)] + [I^-(r)]\} \quad \text{(AII.3)}$$

$$q_{r,P}(r) = \pi \{[I^+(r)] - [I^-(r)]\} \quad \text{(AII.4)}$$

and

$$P_P(r) = \frac{2\pi}{3c} \{[I^+(r)] + [I^-(r)]\} \quad \text{(AII.5)}$$

With this assumption:

$$G_P(r) = 3c P_P(r) \quad \text{(AII.6)}$$

Eq. (AII.6) can be derived with respect to the radial coordinate (r) and substituted into Eq. (AII.2):

$$\underline{\nabla}|_r G_P = -3\beta_P q_{r,P} \quad \text{(AII.7)}$$

Eq. (AII.7) can be derived once more with respect to the radial coordinate (r) and, using Eq. (AII.1), we can get our working equation to solve the problem inside the particle:

$$\nabla^2 \Big|_r G_P = -3\beta_P [\underline{\nabla} \cdot \underline{q_P}]_r = 3(1 - \omega_P) \beta_P^2 G_P \quad \text{(AII.8)}$$

Appendix C

By definition:

$$e_P^a(r) = \underbrace{\kappa_P G_P(r)}_{\text{equivalent to a first order kinetics}} \quad \text{(AIII.1)}$$

In $r = R_p$:

$$e_P^a(R_P) = \kappa_P G_P(R_P) \quad \text{(AIII.2)}$$

Resorting to Eq. (AII.8):

$$\underbrace{\frac{1}{3\beta_P} \nabla^2 \Big|_r G_P}_{\text{attenuation}} = \underbrace{\kappa_P G_P}_{\text{absorption}} \quad \text{(AIII.3)}$$

The first term is equivalent to molecular diffusion in the mass transfer problem, and the second is analogous to a first-order reaction (following the same type of similitude).

From the Eddington approximation (Eq. (AII.7)) and taking into account the existing external surface area per unit volume of the particle:

$$-a_{V_P,ext}q_{r,P}(R_P) = \frac{a_{V_P,ext}}{3\beta_P}\underline{\nabla}G_P|_{R_P} = \underbrace{e^a_{P,eff}}_{\text{effective radiation absorption rate in the particle}} \tag{AIII.4}$$

As it is easily known, for a spherical particle $a_{V_P,ext} = 3/R_P$.

The interpretation of the value of $e^a_{P,eff}$ can be made clearer if one considers the particle as a sink of radiation that is perturbed from an external radiation field. This is the radiation field existing in the suspension at the position where the external surface of the particle is located. According to its optical properties, the said particle may absorb all or part of the incoming radiation flux impinging on its surface.

Recalling Eq. (29) and solving Eq. (AIII.4) it is possible to calculate the value of the effective radiation absorption rate in the particle:

$$e^a_{P,eff} = \frac{1}{\beta_P R_P}(\underline{\nabla}|_r G_P|_{R_P}) = G_P(R_P)\left(\frac{\gamma^2}{\beta_P}\right)\left[\frac{1}{\gamma R_P}\left(\frac{1}{\tanh(\gamma R_P)} - \frac{1}{\gamma R_P}\right)\right] \tag{AIII.5}$$

Defining: $\gamma R_p = 3\gamma^*$ in analogy to the Thiele modulus for mass transfer:

$$e^a_{P,eff} = G_P(R_P)\beta_P(1-\omega_P)\underbrace{\left[\frac{1}{\gamma^*}\left(\frac{1}{\tanh(3\gamma^*)} - \frac{1}{3\gamma^*}\right)\right]}_{\eta^*} \tag{AIII.6}$$

Thus, we can write the relationship existing between the effective radiation absorption rate and $G_P(R_P)$ as follows:

$$e^a_{P,eff} = \underbrace{\kappa_P G_P(R_P)}_{e^a_P(R_P)} \times \eta^* \tag{AIII.7}$$

Eq. (AIII.7) makes clear that:

$$\eta^*(\gamma^*) = \frac{e^a_{P,eff}}{e^a_P(R_p)} = \frac{\text{[LVRPA effectively absorbed inside the particle]}}{\text{[LVRPA absorbed at the surface of the particle]}} \tag{AIII.8}$$

It can be seen that η^* is an efficiency that tell us how operative may be the penetration of the incoming radiation inside the particle to accomplish its objective, i.e., it is a relationship between the total radiation absorbed inside the particle (the LVRPA) with respect to that measured on its external surface where absorption of radiation takes on its maximum value. This value becomes attenuated when the light is penetrating inside the particle according to the optical properties of the latter.

In Eq. (AIII.4) we have defined the value of $e^a_{P,eff}$ from the net radiation flux absorbed by the particle from the external volume of the suspension. An alternative way of defining $e^a_{P,eff}$ can be obtained from the value of the LVRPA existing inside the particle, averaged over its whole volume:

$$e^a_{P,eff} = \frac{4\pi}{V_P}\int_0^{R_P} e^a_P(r)r^2\,dr = \langle e^a_P\rangle_{V_P} \tag{AIII.9}$$

When Eq. (AIII.9) is integrated it gives the same result as Eq. (AIII.6). In this way it can be clearly seen that if the LVRPA inside the particle exhibits a steep radial gradient (a significant attenuation) the particle will not make an efficient use of the available radiation. The opposite occurs when the radiation profiles are smoother. Thus, the efficiency is an exclusive function of the optical thickness, that in the case of the particle is represented by the parameter γ^*.

Appendix D

In order to obtain the relationship between internal and external radiation field, the following balance of fluxes on the particle surface is applied:

$$e^a_{S,ext} = \underbrace{q^-_{r,P}(R_P)}_{\text{in}} - \underbrace{q^+_{r,P}(R_P)}_{\text{out}} = -q_{r,P}(R_P) \tag{AIV.1}$$

Considering the macroscopic properties of the suspension we have:

$$e^a_{S,ext} = \frac{e^a_{susp}}{a_{V,ext}} \tag{AIV.2}$$

where:

$$a_{V,ext} = \frac{A_{P,ext,T}}{V_{susp}} = \frac{A_{p,ext}N_P}{V_{susp}} = \frac{3}{R_P}\frac{m_T}{V_{susp}}\frac{1}{\rho_P} = \frac{3C_{mc}}{R_P\rho_P} \tag{AIV.3}$$

Then:

$$e^a_{S,ext} = \left(\frac{R_P}{3}\right)\left[\frac{\rho_P}{C_{mc}}e^a_{susp}\right] = -q_{r,P}(R_P) \tag{AIV.4}$$

Using Eq. (31) and (AIV.4) we can obtain an expression for the incident radiation on the external surface of the particle as a function of the LVRPA and Eq. (32) in the main text is obtained.

References

[1] M.d.l.M. Ballari, R.J. Brandi, O.M. Alfano, A.E. Cassano, Mass transfer limitations in photocatalytic reactors employing titanium dioxide suspensions. I. Concentration profiles in the bulk, Chem. Eng. J. 136 (2008) 50–65.

[2] A. Sclafani, A. Brucato, L. Rizzuti, Mass transfer limitation in a packed bed photoreactor used for phenol removal, in: D.F. Ollis, H. Al-Ekabi (Eds.), Photocatalytic Purification and Treatment of Water and Air, Elsevier, Amsterdam, 1993, pp. 533–545.

[3] D. Chen, A.K. Ray, Photocatalytic kinetics of phenol and its derivatives over UV irradiated TiO_2, Appl. Catal. B: Environ. 23 (1999) 143–157.

[4] D.D. Dionysiou, M.T. Suidan, I. Baudin, J.M. Laîné, Oxidation of organic contaminants in a rotating disk photocatalytic reactor: reaction kinetic in

the liquid phase and the role of mass transfer based on the dimensionless Damköhler number, Appl. Catal. B: Environ. 38 (2002) 1–16.
[5] K. Mehrotra, G.S. Yablonsky, A.K. Ray, Kinetic studies of photocatalytic degradation in a TiO_2 slurry system: distinguishing working regimes and determining rate dependences, Ind. Eng. Chem. Res. 42 (2003) 2273–2281.
[6] M.F.J. Dijkstra, H.J. Panneman, J.G.M. Winkelman, J.J. Kelly, A.A.C.M. Beenackers, Modeling the photocatalytic degradation of formic acid in a reactor with immobilized catalyst, Chem. Eng. Sci. 57 (2002) 4895–4907.
[7] D. Chen, F. Li, A.K. Ray, Effect of mass transfer and catalyst layer thickness on photocatalytic reaction, AIChE J. 46 (5) (2000) 1034–1045.
[8] M.E. Edwards, C.M. Villa, C.G. Hill, T.W. Chapman, Effectiveness factor for photocatalytic reactions occurring in planar membranes, Ind. Eng. Chem. Res. 35 (1996) 712–720.
[9] G. Camera Roda, F. Santarelli, Effectiveness factor for a photochemical reaction within a plane slab, Chem. Eng. Commun. 19 (1982) 57–66.
[10] C.S. Zalazar, R.L. Romero, C.A. Martín, A.E. Cassano, Photocatalytic intrinsic reaction kinetics i: mineralization of dichloroacetic acid, Chem. Eng. Sci. 60 (2005) 5240–5254.
[11] C.S. Zalazar, Doctoral Thesis, Universidad Nacional del Litoral, 2003.
[12] O.M. Alfano, M.I. Cabrera, A.E. Cassano, Modeling of light scattering in photochemical reactors, Chem. Eng. Sci. 49 (1994) 5327–5346.
[13] C.S. Zalazar, M.D. Labas, C.A. Martín, R.J. Brandi, O.M. Alfano, A.E. Cassano, The extended use of actinometry in the interpretation of photochemical reaction engineering data, Chem. Eng. J. 109 (2005) 67–81.
[14] J. Duderstadt, W. Martin, Transport Theory, Wiley, New York, 1979.
[15] M. Bideau, B. Claudel, L. Faure, H. Kazouan, Diffusional limitations in liquid phase photocatalysis, Prog. React. Kinet. 19 (1994) 195–209.
[16] P.H. Calderbank, M.B. Moo-Young, The continuous phase and mass-transfer properties of dispersions, Chem. Eng. Sci. 16 (1961) 39–54.
[17] M.I. Cabrera, O.M. Alfano, A.E. Cassano, Absorption scattering coefficients of titanium dioxide particulate suspensions in water, J. Phys. Chem. 100 (1996) 20043–20050.
[18] J. Marugán, R. Van Grieken, O.M. Alfano, A.E. Cassano, Optical an physicochemical properties of silica-supported TiO_2 photocatalysts, AIChE 52 (8) (2006) 2832–2843.
[19] C.A. Martín, M.A. Baltanás, A.E. Cassano, Photocatalytic reactors. I. Optical behavior of titanium oxide suspensions, J. Photochem. Photobiol. A: Chem. 76 (1993) 199–208.
[20] G. Imoberdorf, Doctoral Thesis, Universidad Nacional del Litoral, 2006.
[21] M.N. Özisik, Radiative Transfer and Interactions with Conduction and Convection, Wiley, New York, 1973.
[22] K.S. Adzerikho, E.F. Nogotov, V.P. Trofimov, in: Raymond Viskanta (Ed.), Radiative Heat Transfer in Two-Phase Media, English Edition, CRC Press, Inc., Boca Raton, 1993.